

PROTOSTELLAR ACCRETION FLOWS DESTABILIZED BY MAGNETIC FLUX REDISTRIBUTION

RUBEN KRASNOPOLSKY¹, ZHI-YUN LI², HSIEN SHANG¹, BO ZHAO²

Draft version November 12, 2018

ABSTRACT

Magnetic flux redistribution lies at the heart of the problem of star formation in dense cores of molecular clouds that are magnetized to a realistic level. If all of the magnetic flux of a typical core were to be dragged into the central star, the stellar field strength would be orders of magnitude higher than the observed values. This well-known “magnetic flux problem” can in principle be resolved through non-ideal MHD effects. Two dimensional (axisymmetric) calculations have shown that ambipolar diffusion, in particular, can transport magnetic flux outward relative to matter, allowing material to enter the central object without dragging the field lines along. We show through simulations that such axisymmetric protostellar accretion flows are unstable in three dimensions to magnetic interchange instability in the azimuthal direction. The instability is driven by the magnetic flux redistributed from the matter that enters the central object. It typically starts to develop during the transition from the prestellar phase of star formation to the protostellar mass accretion phase. In the latter phase, the magnetic flux is transported outward mainly through advection, by strongly magnetized low-density regions that expand against the collapsing inflow. The tussle between the gravity-driven infall and magnetically driven expansion leads to a highly filamentary inner accretion flow that is more disordered than previously envisioned. The efficient outward transport of magnetic flux by advection lowers the field strength at small radii, making the magnetic braking less efficient and the formation of rotationally supported disks easier in principle. However, we find no evidence for such disks in any of our rotating collapse simulations. We conclude that the inner protostellar accretion flow is shaped to a large extent by the flux redistribution-driven magnetic interchange instability. How disks form in such an environment is unclear.

Subject headings: accretion, accretion disks — magnetic fields — ISM: clouds — stars: formation — magnetohydrodynamics (MHD)

1. INTRODUCTION

Star-forming dense cores of nearby molecular clouds are observed to be significantly magnetized. One line of evidence is the polarization of their submillimeter dust emission (Ward-Thompson et al. 2000), which indicates the existence of an ordered magnetic field on the 0.1 pc scale (e.g., Matthews et al. 2009; Davidson et al. 2011) and smaller (e.g., Girart et al. 2006). Another line of evidence comes from Zeeman measurement. Troland & Crutcher (2008) carried out the most extensive OH Zeeman survey of the dark cloud cores to date with the Arecibo telescope. The measured line-of-sight field strengths (within a beam size of 3′) lie between ~ 10 to $\sim 25 \mu\text{G}$. The inferred mean mass-to-flux ratio is $\lambda_{\text{los}} \sim 4.8$ (in units of the critical mass-to-flux ratio $1/[2\pi G^{1/2}]$, Nakano & Nakamura 1978), based on the measured line-of-sight field strength and column density. Geometric corrections would bring the ratio closer to the critical value, by a typical factor of 2–3 (Shu et al. 2000; Troland & Crutcher 2008). Dense cores therefore appear to be moderately strongly magnetized, with an intrinsic dimensionless mass-to-flux ratio λ of a few to several. Such a magnetic field is too weak to prevent the core from forming one or more stars through gravitational collapse. It is, however, strong enough to affect, even control, the dynamics of the core collapse and protostellar mass accretion, especially the inner part of the protostellar accretion flow that is directly relevant to disk formation.

How rotationally supported disks form around protostars is still uncertain. If an ordered magnetic field of the observationally inferred strength is strictly frozen into the collapsing core material (i.e., in the ideal MHD limit), it would completely suppress the formation of a rotationally supported disk through excessive magnetic braking (Allen et al. 2003; Galli et al. 2006; Mellon & Li 2008; Hennebelle & Fromang 2008; Seifried et al. 2011; Dapp et al. 2012; see, however, Machida et al. 2011, Duffin et al. 2011 and Seifried et al. 2012 for a different view). The reason is that the matter that enters the central object would drag its frozen-in magnetic field into a split-monopole, which is strong enough close to the protostar to brake the rotation of the protostellar accretion flow completely (Galli et al. 2006). Flux-freezing would also lead to the well-known “magnetic flux problem” in star formation, namely, if the magnetic flux of a typical star-forming core is carried into the central star, the stellar field strength would be orders of magnitude higher than the observed values (e.g., Nakano 1984, see his §4). To resolve both problems, the field lines must be allowed to move relative to the bulk matter, i.e., the magnetic flux must be redistributed.

In lightly-ionized dense cores, magnetic flux redistribution can be achieved through non-ideal MHD effects, including ambipolar diffusion, Ohmic dissipation and the Hall effect (e.g., Nakano et al. 2002; Kunz & Mouschovias 2010). Axisymmetric (1D and 2D) calculations have shown that ambipolar diffusion, in particular, can enable the

¹ Academia Sinica, Institute of Astronomy and Astrophysics, Taipei, Taiwan

² University of Virginia, Astronomy Department, Charlottesville, VA, USA

core material to collapse onto the central stellar object without dragging the field lines along (Ciolek & Königl 1998; Krasnopolsky & Königl 2002; Mellon & Li 2009; Li et al. 2011; Braiding & Wardle 2012). The redistributed stellar magnetic flux is trapped instead by the ram pressure of the collapsing flow (Li & McKee 1996), creating a circumstellar region where the flow dynamics is magnetically controlled. In this region, the rotation is nearly completely braked for a realistic level of initial core magnetization (making the formation of rotationally supported disks difficult; Krasnopolsky & Königl 2002; Mellon & Li 2009; Li et al. 2011) and the material in the dense equatorial region becomes magnetically supported (reducing the infall speed well below the local free-fall value). The conclusion from the axisymmetric calculations is that the ambipolar diffusion-enabled redistribution of the magnetic flux that would have entered the protostar in the ideal MHD limit makes the magnetic field dynamically more important outside the central object compared to the ideal MHD case. Similar results were found for Ohmic dissipation and the Hall effect (e.g., Li et al. 2011).

An important issue that has not been fully addressed is the stability of the circumstellar structure produced by the magnetic flux redistribution under the assumption of axisymmetry. It has been suspected for some time that the structure may be prone to the magnetic interchange instability once the axisymmetry is removed, because the region close to the protostar is expected to be more strongly magnetized than farther out (Li & McKee 1996, see their Fig. 1; Ciolek & Königl 1998; Krasnopolsky & Königl 2002). The criterion for the interchange instability is that the mass-to-flux ratio decreases in the direction of gravity in the simplest case of a magnetically supported, non-rotating sheet (Spruit & Taam 1990). This criterion is formally satisfied in part of the 1D (axisymmetric) ambipolar diffusion-mediated accretion flow studied by Ciolek & Königl (1998). However, the development of the expected instability has never been explored in detail using 3D non-ideal MHD simulations. It is the goal of this paper.

Our non-ideal MHD simulations will build on the work of Zhao et al. (2011), who investigated the collapse of magnetized cores and protostellar accretion using an ENZO-based ideal MHD code (Wang & Abel 2009). The magnetic flux redistribution is achieved through a sink particle treatment. When the mass in a cell is accreted onto a sink particle, the magnetic field is left behind in the cell (see also Seifried et al. 2011); the treatment is a crude representation of the field-matter decoupling expected at high densities (of order 10^{12} cm^{-3} or higher; Nakano et al. 2002; Kunz & Mouschovias 2010). The decoupled magnetic flux piles up near the sink particle, leading to a high magnetic pressure that is released through the escape of field lines along the directions of least resistance. The net result is that the magnetic flux dragged into the decoupling region near the protostar along some azimuthal directions by the collapsing flow is advected back out along other directions in highly magnetized, low-density, expanding regions. The main effects of the magnetic flux redistribution on the protostellar accretion flow are (1) the co-existence of the magnetically driven expansion and gravitationally driven infall, which makes the flow more disordered than previously envisioned, and (2) advective transport of the redistributed magnetic flux to large distances, which is absent under the assumption of axisymmetry. We show in this paper that these two basic features are preserved in the presence of the two most widely studied non-ideal MHD effects in star formation: ambipolar diffusion and Ohmic dissipation.

2. PROBLEM SETUP

Following Krasnopolsky et al. (2010; 2011) and Li et al. (2011), we start our simulations from a uniform, spherical core of $1 M_{\odot}$ and radius 10^{17} cm . The initial density is therefore $\rho_0 = 4.77 \times 10^{-19} \text{ g cm}^{-3}$, corresponding to a molecular hydrogen number density of 10^5 cm^{-3} . We adopt an isothermal equation of state, with a sound speed $a = 0.2 \text{ km s}^{-1}$, up to a critical density $\rho_c = 10^{-13} \text{ g cm}^{-3}$. Beyond ρ_c , a polytropic equation of state $p \propto \rho^{5/3}$ is adopted. At the beginning of the simulation, we impose a uniform magnetic field of $B_0 = 35.4 \mu\text{G}$. It corresponds to a dimensionless mass-to-flux ratio of $\lambda = 2.92$ for the core as a whole (and a plasma β of 3.82 for the adopted isothermal sound speed), which is in the observationally inferred range (see §1). The mass-to-flux ratio for the central flux tube is 4.38, higher than the global value by 50%. We have experimented with magnetic fields as weak as $3.54 \mu\text{G}$, and found qualitatively similar results.

For illustrative purposes, we adopt the simplified treatment of ambipolar diffusion of Shu (1992, Chapter 27), with the magnetic field tied to the ions and the ion density proportional to the square root of the mass density. The proportionality constant scales with $\zeta^{1/2}$, where ζ is the cosmic ray ionization rate. We will consider the canonical value $\zeta = 10^{-17} \text{ s}^{-1}$, although there is evidence for higher values in star-forming clouds (e.g., Padovani et al. 2009). Our reference model will have $\zeta = 9 \times 10^{-17} \text{ s}^{-1}$, which contains three times more ions than in the canonical case. In addition, we will consider cases with a spatially constant resistivity $\eta = 10^{17} \text{ cm}^2 \text{ s}^{-1}$. The value is larger than the classical microscopic resistivity at the densities encountered in our simulations (see Li et al. 2011). It is chosen to illustrate the effects of Ohmic dissipation while minimizing the violent numerical reconnection that dominates the protostellar accretion simulations in the ideal MHD limit (e.g., Mellon & Li 2008). We also consider cases where a relatively large resistivity of $\eta = 10^{19} \text{ cm}^2 \text{ s}^{-1}$ is assumed within a small radius of $2 \times 10^{14} \text{ cm}$ of the central object, to illustrate the effects of magnetic decoupling (see §4.3). In some cases, we include an initial solid-body rotation of angular speed $\Omega_0 = 10^{-13} \text{ s}^{-1}$ in the core, to study the possibility of disk formation. It corresponds to a ratio of rotational to gravitational binding energy of 0.025, which is typical of the values inferred for NH_3 cores (Goodman et al. 1993). The models to be discussed in the result sections (§3 and §4) are listed in Table 1.

Our 3D non-ideal MHD simulations were carried out in the coordinate system most natural for the collapse problem: the spherical polar system (r, θ, ϕ) . Both the initial magnetic field and rotation directions are along the $\theta = 0$ axis. We choose a non-uniform grid of $96 \times 64 \times 60$. In the radial direction, the inner and outer boundaries are located at $r = 10^{14}$ and 10^{17} cm , respectively. The radial cell size is smallest near the inner boundary ($5 \times 10^{12} \text{ cm}$ or $\sim 0.3 \text{ AU}$).

TABLE 1
PARAMETERS OF 3D NON-IDEAL MHD MODELS

Model	ζ (10^{-17} s^{-1})	η ($\text{cm}^2 \text{ s}^{-1}$)	Ω_0 (10^{-13} s^{-1})	Central object ^a
A	9	0	0	after
B	9	0	0	before
C	9	0	1	before
D	1	0	0	before
E	no AD	spatially uniform, 10^{17}	0	before
F	no AD	spatially uniform, 10^{17}	1	before
G	no AD	step function, 1 & 10^{19}	0	before
H	no AD	step function, 1 & 10^{19}	1	before
I	9	step function, 1 & 10^{19}	0	before
J	9	step function, 1 & 10^{19}	1	before

NOTE. — a). The 3D simulations are restarted from their corresponding 2D (axisymmetric) simulations either before or after the formation of an object of significant mass at the center.

It increases outward by a factor of 1.08 between adjacent cells. In the polar direction, we choose a relatively large cell size (7.5°) near the polar axes, to prevent the azimuthal cell size from becoming prohibitively small, because the time step must be proportional to the cell size squared to ensure numerical stability for our explicit treatment of the non-ideal MHD effects, particularly ambipolar diffusion. The polar cell size decreases smoothly to a minimum of 0.63° near the equator, where most of the protostellar mass is accreted, through the “pseudo-disk” (Galli & Shu 1993). The grid is uniform in the azimuthal direction, with the cell size equal to 6 degrees. For our reference model (Model B in Table 1), we have increased the number of azimuthal cells to 90 and 120, and found qualitatively similar results.

The boundary conditions in the azimuthal direction are periodic. In the radial direction, we impose the standard outflow boundary conditions. Material leaving the inner radial boundary is collected as a point mass (protostar) at the center. It acts on the matter in the computational domain through gravity. On the polar axes, the boundary condition is chosen to be reflective (as in the 2D axisymmetric case). Although this is not strictly valid in 3D, we do not expect it to affect much the dynamics of the equatorial region, through which most of the mass accretion onto the central protostar occurs. In order to speed up the simulations, a density floor is utilized. It is set up so that the Alfvénic time step is not smaller than $3 \times 10^5 \text{ s}$. This is a reasonable value in a simulation that reaches more than $4 \times 10^{12} \text{ s}$. For similar reasons, the coefficient of ambipolar diffusion is capped so that its time step is not smaller than 10^6 s . In the inner parts of the simulation ($r < 1.5 \times 10^{15} \text{ cm}$) an additional density floor is set at the relatively low value of $2 \times 10^{-19} \text{ g cm}^{-3}$. We monitored the mass added through the use of the density floors and Alfvénic time step limiter and found it to be insignificant.

We treat the self-gravity by extending the method of successive over-relaxation (SOR) used in the two-dimensional (axisymmetric) core collapse calculations of Li et al. (2011) to 3D (see also Ramsey et al. 2012). In 2D, the boundary condition for the gravitational potential was obtained by direct summation. This proved to be too expensive in 3D, however. We employed instead the method of multipole expansion (with degree $l = 5$) to determine the boundary condition on a grid extended by 10 zones in both the inner and outer radial directions. The new grid extends from $r = 5 \times 10^{13}$ to $2 \times 10^{17} \text{ cm}$.

3. STABILITY OF AXISYMMETRIC, AMBIPOLAR DIFFUSION-MEDIATED PROTOSTELLAR ACCRETION FLOWS

Ambipolar diffusion is the most widely studied non-ideal MHD effect in star formation, because it dominates other non-ideal effects at densities typical of dense cores. It allows the magnetized core matter to collapse onto the central object without dragging the field lines along, as discussed in §1. Previous 2D (axisymmetric) calculations have shown that the redistributed magnetic field piles up in a small circumstellar region, and becomes increasingly dynamically dominant there (see, e.g., Li et al. 2011). This situation is illustrated in Fig. 1, which shows the infall speeds in the equatorial region during the collapse of a non-rotating, magnetized ($\lambda = 2.92$) core, in the presence of ambipolar diffusion ($\zeta = 9 \times 10^{-17} \text{ s}^{-1}$). The time shown is $t = 4.25 \times 10^{12} \text{ s}$, when $0.12 M_\odot$ has been accreted onto the central object. It is clear that the equatorial infall is decelerated to a speed much smaller than the local free-fall speed inside a radius of roughly $4 \times 10^{14} \text{ cm}$ (corresponding to the hydromagnetic shock first studied by Li & McKee 1996, see §1), where the redistributed magnetic flux accumulates. In this decelerated region, the material is held up against the gravity by magnetic forces, a situation that is prone to instability in 3D.

To investigate the stability of the magnetically supported structure induced by ambipolar diffusion in the accretion flow, we restart, in 3D, the 2D calculation at the time shown in Fig. 1, when a central object of $0.12 M_\odot$ has already formed (Model A in Table 1). We find that the axisymmetry is broken quickly, with regions of outward motion first developing near the inner boundary and then expanding to larger distances. After a relatively short time of $2 \times 10^{10} \text{ s}$, the expansion reaches a size of order $2 \times 10^{15} \text{ cm}$ (20 times the radius of the inner boundary), as shown in Fig. 2, where the density distribution and velocity field on the equatorial plane are plotted. The figure shows that the expansion is confined mostly to low-density lobes. These evacuated lobes are filled with a relatively strong magnetic field, as illustrated in Fig. 3, where we show the distribution of the total field strength and the mass density along the positive x -axis in Fig. 2 (with $\theta = \pi/2$ and $\phi = 0$, cutting through the right lobe). In the low density region (between radius

$\sim 4 \times 10^{14}$ and $\sim 2 \times 10^{15}$ cm), the dynamics is completely dominated by a strong, nearly uniform magnetic field, with a strength ($\sim 10^{-2}$ G) much larger than at larger radii (outside the magnetically dominated lobe). The increase in field strength at small radii is associated with the dense filaments inside the right lobe that are visible in Fig. 2. We have verified that the magnetic pressures in the evacuated lobes are large enough to overwhelm the ram pressure of the infalling material. The pressure imbalance is the reason for the observed expansion in those directions. The expanding lobes are reminiscent of the so-called “decoupling enabled magnetic structure” (DEMS) found by Zhao et al. (2011) in their 3D ideal-MHD AMR simulations of core collapse including sink particles. As in Zhao et al. (2011), the dense structures surrounding the expanding regions are ring-like rather than shell-like in 3D (see their Fig. 3); they are created out of the dense equatorial pseudo-disk that is already highly flattened to begin with (see the top-right panel of Fig. 4 below).

We have carried out several variants of the above model, including models with either a ten times weaker initial magnetic field, a nine times lower rate of cosmic ray ionization, or a non-zero initial rotation rate. The results are qualitatively similar, namely, the initially axisymmetric inner protostellar accretion flow quickly becomes unstable in the azimuthal direction in 3D. An implication is that the assumed smooth protostellar accretion flow is unlikely to be achievable in the first place. We now demonstrate that this is indeed the case.

4. UNSTABLE PROTOSTELLAR ACCRETION FLOWS

4.1. Reference Model

We have restarted the above calculation (Model A) in 3D from the very beginning ($t = 0$), when the core is assumed to be a uniform sphere. We find that the core remains axisymmetric during most of the (long) prestellar evolution. To save computation time, we skip the uneventful early part of the prestellar core evolution, and restart most of our 3D calculations from 2D calculations shortly before a central object of significant mass has formed and any visible asymmetry has developed. In this subsection, we will concentrate on a representative of such models, the Model B in Table 1, which serves as a reference for the other models to compare with. This model is identical to Model A discussed above, except that we restart the 3D collapse calculation from the 2D collapse at an earlier time of $t = 4.12 \times 10^{12}$ s, when the central object contains only a tiny mass of $2.72 \times 10^{-5} M_{\odot}$ (much smaller than the $0.12 M_{\odot}$ in Model A). We find that the magnetized collapsing flow starts to become visibly asymmetric during the transition between the prestellar phase of core evolution to the protostellar phase of mass accretion, when the mass accretion rate onto the central object increases rapidly. During the protostellar accretion phase, matter continues to collapse onto the central protostar in some azimuthal directions, while the magnetic flux dragged in by the accretion flow escapes in the other directions, driving outward motions against the inward collapse. The filamentary structure resulting from the tussle between the gravity-driven inflow and the flux escape-driven expansion is illustrated in the top-left panel of Fig. 4, where we plot the density distribution and velocity field on the equatorial plane at a time $t = 4.22 \times 10^{12}$ s, when $0.092 M_{\odot}$ has collapsed into the central object. As emphasized earlier, the high density regions shown in the panel are not parts of dense shells. Rather, they are filaments that lie near the equatorial plane (see the top-right panel of

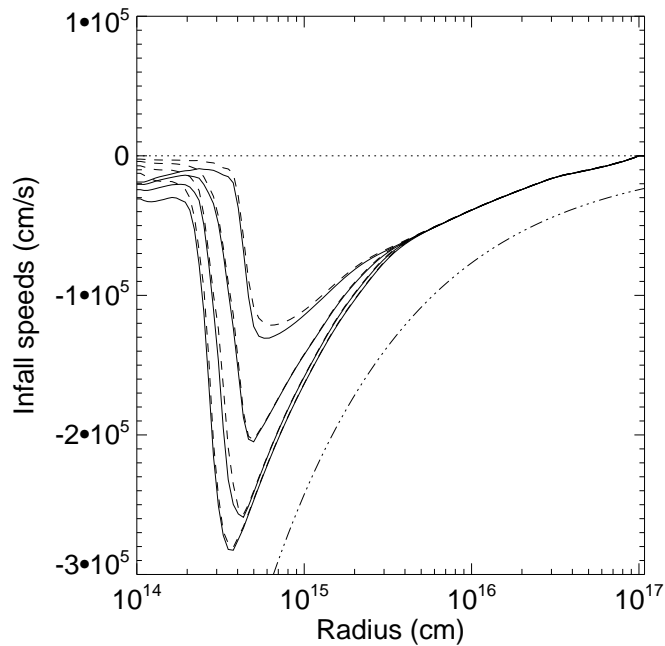


FIG. 1.— Infall speeds in the equatorial region of a representative 2D (axisymmetric) protostellar accretion flow in the presence of ambipolar diffusion, along four radial directions that are (from top to bottom) 0.31, 0.97, 1.68 and 2.44 degrees from the equatorial plane. The ion and neutral speeds are plotted as dashed and solid lines, respectively. The free fall speed is plotted for reference (dashed-dotted).

Fig. 4), as part of the magnetically flattened pseudo-disk that would have formed in 2D but is disrupted in 3D by the escaping bundles of magnetic field lines. The flow morphologies displayed in these two panels illustrate the highly dynamic nature of the inner (10^2 AU-scale) protostellar accretion flows that form out of the collapse of dense cores magnetized to the observed level. The dynamic nature can be seen more vividly in the movies that can be requested from the authors.

It should not be surprising that the magnetic field is dynamically important in the inner part of the protostellar accretion flow. In the bottom two panels of Fig. 4, we plot the plasma β (the ratio of thermal to magnetic pressures)

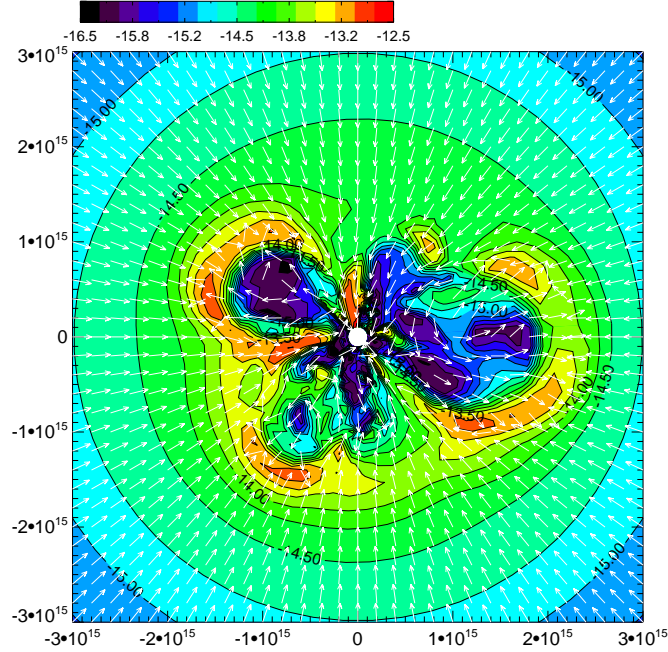


FIG. 2.— Distribution of the logarithm of the mass density ρ (in g cm^{-3}) and velocity field (unit vectors) on the equatorial plane, at a representative time for Model A, which is restarted from the 2D (axisymmetric) calculation at the time shown in Fig. 1. The length unit is cm.

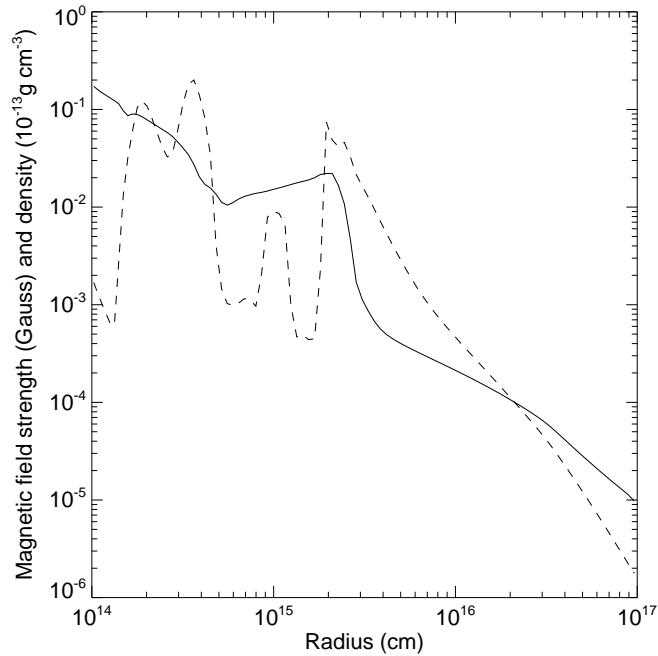


FIG. 3.— Distribution of the total magnetic field strength (solid line) and mass density (in units of $10^{-13} \text{ g cm}^{-3}$, dashed) along the positive x -axis in Fig. 2.

on the equatorial plane and a representative meridian plane (along $\phi = 0$ and π). It is clear from the bottom-right panel that the vast majority of the volume on the 10^2 AU scale is filled with low- β plasma, as a result of the increase in field strength due to collapse-induced compression and mass settlement along the field lines into the pseudo-disk in the equatorial region. Even on the equatorial plane, most of the area is covered by strongly magnetized material with $\beta \ll 1$ within a radius of 10^2 AU at the time shown, although there are “fingers” of less strongly magnetized material with $\beta \sim 1$ (see the bottom-left panel). It is these dense, less magnetized “fingers” or “filaments” that dominate the mass accretion onto the central object, which is at a rate of $\sim 3 \times 10^{-5} M_{\odot} \text{ yr}^{-1}$ at the time shown. The infall material percolates through a “sea” of highly magnetized, low-density medium.

It is instructive to compare the 3D simulation shown in Fig. 4 more quantitatively to the 2D version of the simulation at the same time ($t = 4.22 \times 10^{12}$ s). One fundamental difference between the 3D and 2D models is how the magnetic flux is transported. In the top-left panel of Fig. 5, we display the rate of magnetic flux transport, $\dot{\Phi}$, across a circle C

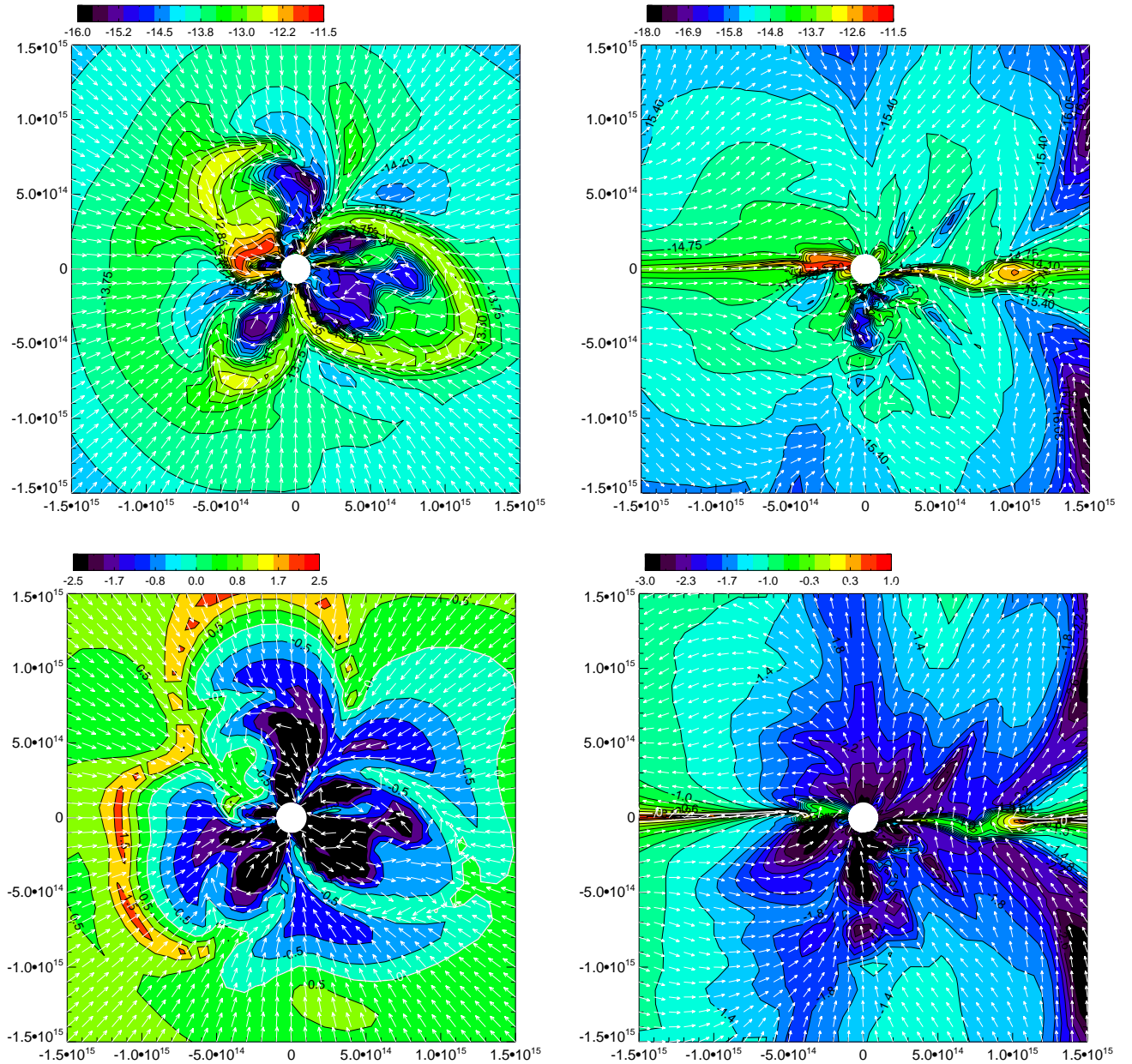


FIG. 4.— Distribution of the logarithm of the mass density ρ and velocity field (unit vectors) on the equatorial plane (top-left panel) and a representative meridian plane (top-right) for Model B, at a time when the central mass is $0.092 M_{\odot}$. The bottom panels show the distribution of the logarithm of the plasma- β on the equatorial plane (left, with velocity unit vectors superposed) and the representative meridian plane (right, with magnetic unit vectors superposed). The white contours in the two panels mark $\beta = 1$.

of radius r and circumference ∂C on the equatorial plane, computed as

$$\dot{\Phi}_i \equiv \frac{\partial \Phi}{\partial t} = - \int_C \frac{\partial \mathbf{B}}{\partial t} \cdot d\mathbf{S} = \int_C \nabla \times (\mathbf{B} \times \mathbf{v}_i) \cdot d\mathbf{S} = \int_{\partial C} (\mathbf{B} \times \mathbf{v}_i) \cdot d\ell = \int_0^{2\pi} (B_r v_{\theta,i} - B_{\theta} v_{r,i}) r d\phi \quad (1)$$

where the subscript ‘‘i’’ stands for ions, which are assumed to be well coupled to the magnetic field, $d\mathbf{S}$ and $d\ell$ are area and length vector elements, and Φ is the flux.³ For comparison, we also compute the rate of flux transport associated with the neutral velocity $\dot{\Phi}_n$; it is the expected rate in the absence of ambipolar diffusion. We find that, in 2D, the bulk neutral material would have dragged in magnetic flux at a high rate (the dot-dashed line in the panel) at small radii were it not for ambipolar diffusion. The ion-neutral drift reduces the rate greatly, especially close to the inner boundary (see the dotted line). In contrast, the ion-neutral drift is much less effective in reducing the rate of inward magnetic flux transport in 3D (mostly by infalling material), as seen from the small separation between the bottom solid and dashed lines. Most of the magnetic flux carried in by the infalling neutral material is advected back out by the low-density expanding material; the outward flux advection is not modified by ambipolar diffusion much either (note the small separation between the top solid and dashed lines). The conclusion is that, in 3D, the magnetic transport is dominated by advection through bulk fluid motions, with ambipolar diffusion playing a much reduced role compared to the 2D case. We will return to this important conceptual point in the discussion section (§5.2).

The different modes of magnetic flux transport in 2D and 3D have profound effects on the dynamics of the protostellar accretion flow. In the remaining three panels of Fig. 5, we compare the azimuthally averaged radial distributions of the vertical field strength, mass density, and infall speed on the equatorial plane for the 2D and 3D models. It is clear that the magnetic field is more concentrated at small radii in 2D than in 3D (see the top-right panel), because the microscopic ambipolar diffusion in 2D is less efficient in smoothing out the field concentration than the macroscopic flux advection in 3D. The reduction in the field concentration is the main reason why ambipolar diffusion plays a reduced role in the magnetic flux transport in 3D, as pointed out above. The reduction in magnetic field strength and the associated magnetic forces in 3D enables the accretion flow to collapse faster toward the central object (see the bottom-right panel), which in turn leads to lower densities at small radii (see the bottom-left panel). In 3D, a larger region is affected by the accreted magnetic flux, which is more widely redistributed.

4.2. Rotation, Ionization Level, and Ohmic Dissipation

Unstable, filamentary protostellar accretion is not unique to the reference model (Model B) that includes ambipolar diffusion. We have carried out dozens of runs with different model parameters and different non-ideal MHD effect (Ohmic dissipation), and they all show a qualitatively similar behavior. Fig. 6 displays four examples. In the top-left panel, we plot the velocity field and density distribution on the equatorial plane of a case that is identical to the reference run except for the initial rotation rate, which is now $\Omega = 10^{-13} \text{ s}^{-1}$ rather than zero (Model C in Table 1). The counter-clockwise rotation can be seen in the panel. It does not fundamentally change the filamentary morphology of the accretion flow. In particular, a rotationally supported disk (RSD) has not formed up to the time shown ($t = 4.575 \times 10^{12} \text{ s}$), which corresponds to a relatively early phase of protostellar mass accretion, when the central mass is only $0.071 M_{\odot}$. We were unable to run the simulation much longer because of numerical difficulties associated with strong magnetic fields in low density regions. The top-right panel displays Model D, which is identical to the reference Model B, except for the cosmic ray ionization rate, which now has the canonical value $\zeta = 10^{-17} \text{ s}^{-1}$ instead of $9 \times 10^{-17} \text{ s}^{-1}$. The snapshot is taken at time $t = 4.163 \times 10^{12} \text{ s}$, when the central mass is $0.096 M_{\odot}$. Again, we find filamentary structures shaped by the interplay between gravitational infall and the magnetically driven expansion.

The unstable, filamentary accretion is not limited to magnetized collapse in the presence of just ambipolar diffusion. In the bottom panels of Fig. 6, we show two representative models with a spatially constant resistivity of $\eta = 10^{17} \text{ cm}^2 \text{ s}^{-1}$; this value is larger than the classical microscopic value for the density range under consideration, and is adopted for illustrative purposes only. We have experimented with $\eta = 10^{16}$ and $10^{18} \text{ cm}^2 \text{ s}^{-1}$ and found qualitatively similar results. The adopted resistivity has the advantage of enabling the simulations to run longer in the protostellar mass accretion phase compared to the ambipolar diffusion cases. The bottom-left panel shows a non-rotating case that is the same as the reference model, except that ambipolar diffusion is now replaced by Ohmic dissipation (Model E), at a time $t = 4.5 \times 10^{12} \text{ s}$, when $0.22 M_{\odot}$ of mass has been accreted onto the central object. By this time, the filamentary accretion region has expanded beyond $\sim 4 \times 10^2 \text{ AU}$. The last panel displays a case that is the same as Model E, except that the core rotates initially with an angular speed of $\Omega = 10^{-13} \text{ s}^{-1}$ (Model F in Table 1). As in the ambipolar diffusion case, there is no hint of the formation of a rotationally supported disk out of the collapse of the rotating core, even at the rather late time shown ($t = 4.82 \times 10^{12} \text{ s}$), when the central mass has grown to $0.16 M_{\odot}$. We conclude that protostellar accretion flows are unstable and become filamentary in the presence of a moderate level of Ohmic dissipation, with or without rotation, as is true for the models with ambipolar diffusion.

4.3. Magnetic Decoupling and Nature of the Instability

The magnetic field is expected to decouple from the bulk neutral material sooner or later as the density increases, because the gas becomes less ionized and the charged particles less well tied to the field lines. The exact value for the decoupling density is somewhat uncertain. Nakano et al. (2002) estimated a value of a few times 10^{11} cm^{-3} . It

³ The four equal signs in equation (1) are justified based on the definition of magnetic flux, the induction equation, Stokes’ theorem, and expansion on spherical coordinates, respectively. The definition of magnetic flux is based on $B_z = -B_{\theta}$.

may however be an order of magnitude higher according to Kunz & Mouschovias (2010). Treating the decoupling fully would require a detailed calculation of the number densities of all charged species (including dust grains), which is beyond the scope of this work. Nevertheless, as long as the decoupling occurs at a high enough density (or close enough to the origin, as found by Nakano et al. 2002 and Kunz & Mouschovias 2010), the essence of the process is already captured in our simulations, through the use of an inner radial boundary at $r = 10^{14}$ cm (or 6.7 AU): matter that crosses the boundary is accreted onto the central object, and becomes decoupled from the magnetic field lines that were originally attached to the matter but are now left behind in the computational domain. The basic features of the protostellar accretion flow do not depend on the size of the inner boundary. For example, we have shrunk that size by a factor of 2 for Model B and E, and found that the flow pattern remains qualitatively similar.

The models discussed so far rely on the use of an inner boundary for treating the magnetic decoupling. In Models G and H of Table 1, we refine the treatment by including a small diffusive region outside the inner boundary. It is done through a step function for the resistivity, with $\eta = 10^{19}$ cm² s⁻¹ inside $r_c = 2 \times 10^{14}$ cm (twice the radius of

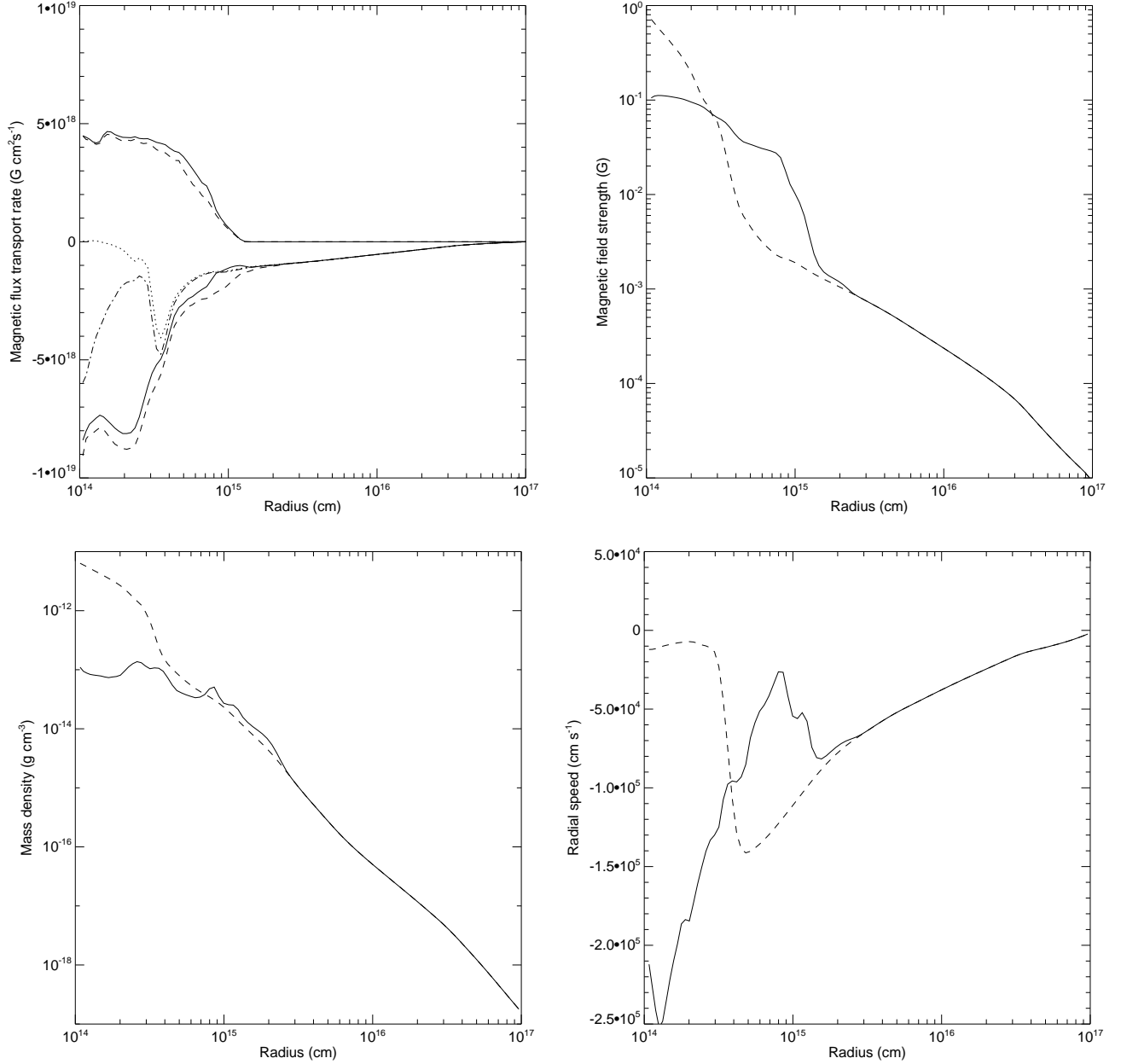


FIG. 5.— Top-left panel: rates of magnetic flux transport (see equation 1) associated with the ion ($\dot{\Phi}_i$, solid lines) and neutral ($\dot{\Phi}_n$, dashed) velocities across circles of different radii on the equator for (3D) Model B. The bottom and top pairs of lines are for the inward and outward flux transport, respectively. The rates of flux transport associated with the ion (dotted line) and neutral (dot-dashed) velocities in 2D are also shown for comparison. The remaining panels compare the azimuthally averaged radial distributions of the vertical field strength (top-right panel), mass density (bottom-left), infall speed weighted by mass (bottom-right) on the equatorial plane for the 3D (solid lines) and 2D (dashed) models.

the inner boundary), and $\eta = 1 \text{ cm}^2 \text{ s}^{-1}$ outside. The outside resistivity is so small that the field lines are essentially frozen in the matter. Inside r_c , one would ideally like to choose an η as large as possible, so that the magnetic field is completely decoupled from the matter and can thus be easily redistributed relative to the matter. However, the larger the resistivity η is, the smaller the time step dt must be in order to ensure numerical stability for our explicit treatment of the Ohmic dissipation. As a compromise, we settled on a value $\eta = 10^{19} \text{ cm}^2 \text{ s}^{-1}$, which is large enough to illustrate the effects of magnetic decoupling but small enough that the simulation can be completed in a reasonable amount of time. We also increased the critical density for stiffening the equation of state by a factor of 10^3 , to $\rho_c = 10^{-10} \text{ g cm}^{-3}$, so that the accretion flow remains isothermal, which makes it easier to see how the magnetic flux redistribution-driven instability develops.

The evolution of Models G and H is illustrated in Fig. 7, which shows snapshots of the density and field strength distributions on the equatorial plane at three representative times. We will concentrate on the non-rotating Model G first. At the earliest time shown ($t = 4.205 \times 10^{12} \text{ s}$), the accretion flow remains nearly axisymmetric. The most striking feature is that the strength of the magnetic field inside the resistive region (within radius $r_c = 2 \times 10^{14} \text{ cm}$) is more than an order of magnitude higher than that outside (top row, second column). This is because magnetic flux

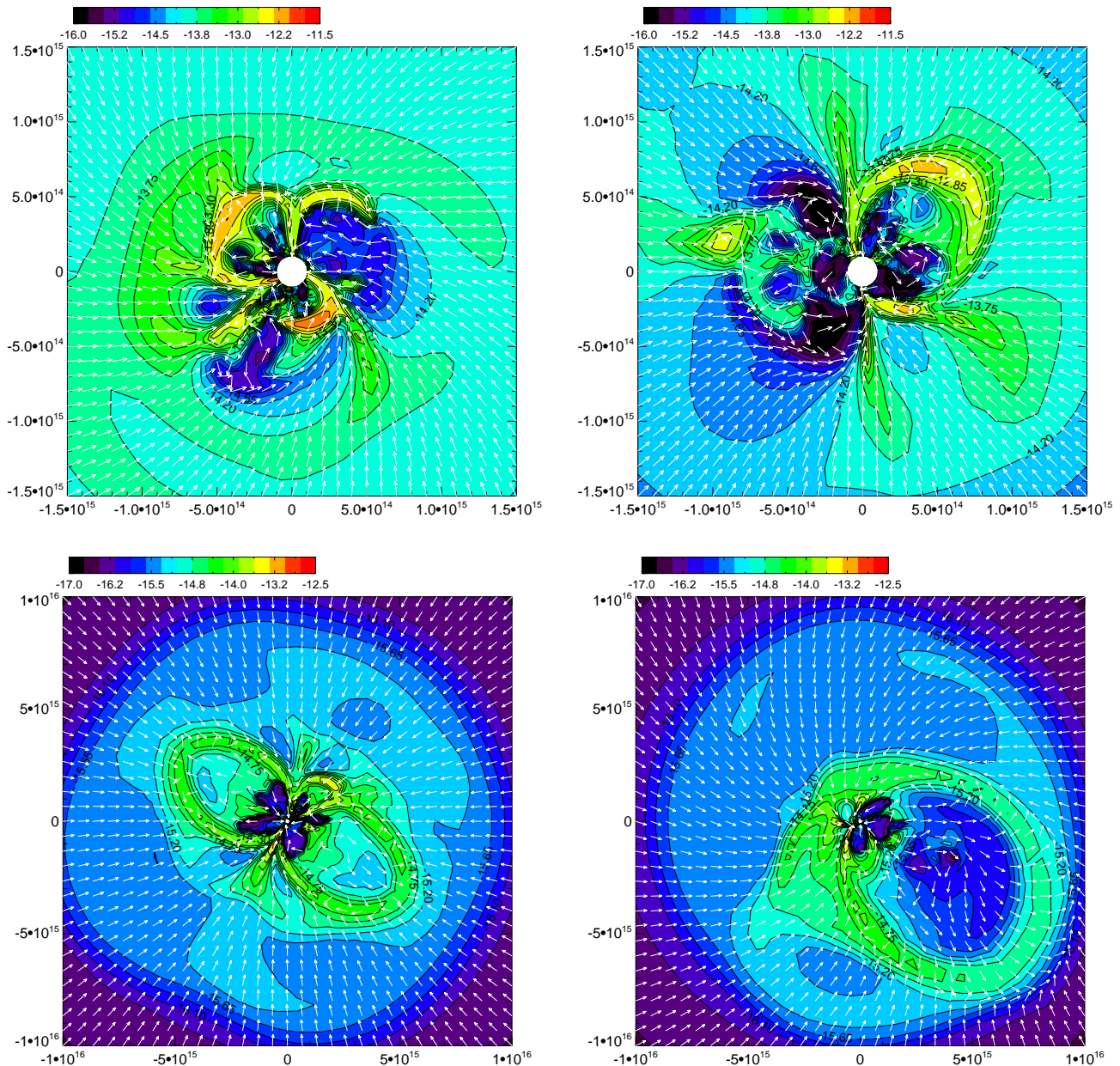


FIG. 6.— Distribution of the logarithm of the mass density ρ and velocity field (unit vectors) on the equatorial plane, for Models C (top-left panel), D (top-right), E (bottom-left) and F (bottom right), all showing filamentary structures in the inner protostellar accretion flow. Note the change in size scale between the top and bottom panels.

is dragged into the resistive region by accretion, and this magnetic flux is not destroyed by the large local resistivity, despite occasional claims to the contrary in the literature; rather, it accumulates in the resistive region. At the time shown in the top panels, the accumulated magnetic flux is $\Phi_c = 4.95 \times 10^{28} \text{ G cm}^2$. The total mass inside the region is $M_c = 9.16 \times 10^{31} \text{ g}$, with most of the contribution coming from the central mass, which has $8.82 \times 10^{31} \text{ g}$. The dimensionless mass-to-flux ratio for the region is therefore $\lambda_c = 3.00$, which is close to the average value for the dense core as a whole (2.92), indicating that the magnetic flux associated with the mass that has entered the central object is indeed trapped in the resistive region. The value $\lambda_c = 3.00$ is somewhat smaller than the initial value on the central flux tube (4.38), as expected, because not all of the matter along the redistributed field lines has collapsed into the resistive region.

The rapid increase in field strength across the boundary r_c between the nearly ideal MHD and resistive region implies a large magnetic pressure gradient near r_c , which opposes the local gravitational collapse. The magnetic pressure force is aided by the magnetic tension force near the boundary, where the poloidal field lines become highly pinched. The net effect is a rapid deceleration of the collapsing flow near the boundary, which leads to a local pile-up of material. The pile-up corresponds to the density peak near r_c (see the top-left panel). Inside r_c , the magnetic field is less well coupled to the matter, which allows the gravity to re-accelerate the gas to high speed and thus lower the density.

The magnetically supported region becomes unstable in the azimuthal direction shortly afterward, with high frequency modes dominating initially (see the middle row, left two panels). This is characteristic of magnetic interchange instability, and has been seen, for example, in the simulations of accretion disks threaded by a strong magnetic field by Stehle & Spruit (2001). In the absence of rotation, Spruit & Taam (1990) find that the criterion for the instability is that the mass-to-flux ratio decreases in the direction of the gravity. This condition is satisfied in our case because of the magnetic flux redistribution inside the resistive region, which reduces the mass-to-flux ratio inside the region compared to that outside.

As the interchange instability grows, lower frequency azimuthal modes are expected to become more prominent (see, e.g., Fig. 3 of Stehle & Spruit 2001). This is indeed the case for our model, as shown in the bottom row (left two

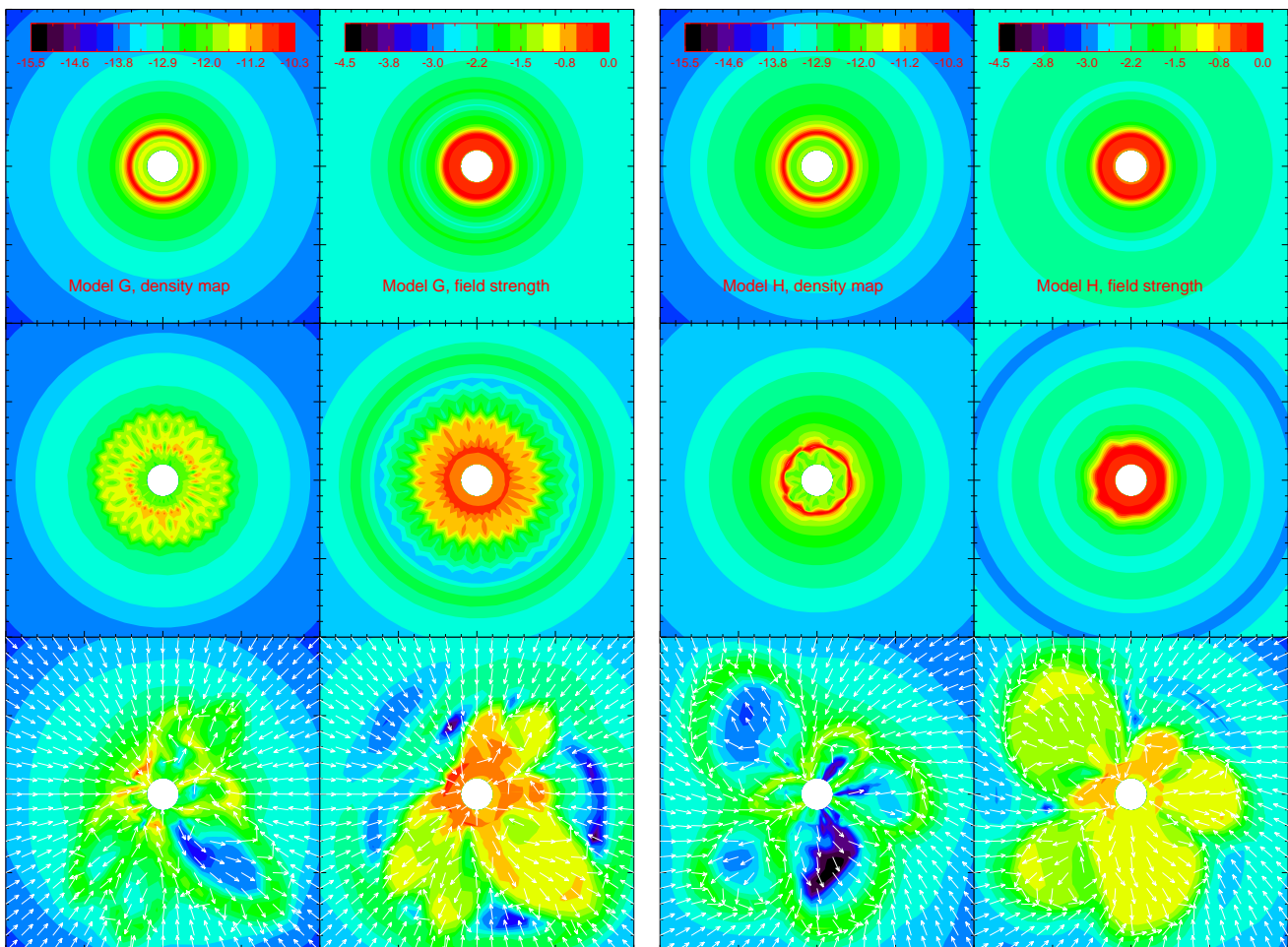


FIG. 7.— Evolution of Model G (non-rotating, left two columns) and H (rotating, right two columns), at three representative times (from top to bottom). The first and third columns show the equatorial density distribution for Model G and H respectively, and the second and fourth columns show the distribution of the component of magnetic field perpendicular to the equator ($B_z = -B_\theta$) for Model G and H. In both models, the redistribution of magnetic flux inside the resistive region gives rise to interchange instability that leads to advective magnetic flux transport, as indicated by the (unit) velocity vectors shown in the bottom panels. The size of each panel is $2 \times 10^{15} \text{ cm}$.

columns) of Fig. 7, where the distributions of the density and magnetic field strength are dominated by several lobes, especially the one along the lower-right direction. This lobe grows preferentially relative to the others. It dominates the dynamics of the inner accretion flow at later times.

The evolution of Model H with rotation (the right two columns of Fig. 7) is similar to the non-rotating Model G. Magnetic flux is again trapped in the resistive region, which leads to interchange instability. The instability develops more gently compared to the non-rotating case, presumably because it is weakened somewhat by differential rotation, as predicted from the linear analysis (Lubow & Spruit 1995). The rotation does not fundamentally change the nonlinear outcome of the instability, however. In both cases, lobes of highly magnetized material expand away from the origin, transporting magnetic flux to large distances well outside the small resistive region. We conclude that the field-matter decoupling in the resistive region has driven the inner protostellar accretion flow unstable, which leads to the new mode of advective magnetic flux transport that does not depend on local microscopic magnetic diffusion and that operates even in the ideal MHD part of the flow. This is in agreement with the ideal MHD simulations of Zhao et al. (2011), where the magnetic decoupling is represented with a sink particle treatment.

In Models I and J, we repeat Model G and H, but include ambipolar diffusion with a cosmic ray ionization rate of $\zeta = 9 \times 10^{-17} \text{ s}^{-1}$ (see Table 1). These are the most comprehensive of our simulations, because they include both ambipolar diffusion that is important at relatively low densities and Ohmic dissipation that is thought to play a crucial role in the magnetic decoupling at high densities (Nakano et al. 2002). The results are illustrated in Fig. 8. The left panel shows the non-rotating Model I at a time $t = 4.32 \times 10^{12} \text{ s}$, when the central mass is $0.162 M_{\odot}$. The right panel displays the rotating Model J at $t = 4.67 \times 10^{12} \text{ s}$, when the central mass is $0.129 M_{\odot}$. In both cases, the flow morphology is dominated by expanding lobes along some azimuthal directions and infall along others, broadly similar to the features present in all other models. The similarity reinforces the notion that these are robust features that are insensitive to the detailed treatment of the magnetic decoupling, the nature of the microscopic magnetic diffusion (ambipolar diffusion or Ohmic dissipation), or rotation.

5. DISCUSSION AND SUMMARY

5.1. Magnetic Domination of Inner Protostellar Accretion Flow

A general result that we find is that the magnetic field dominates the dynamics of the inner protostellar accretion flow out to hundreds of AU (see, e.g., Fig. 4), even though its initial strength is relatively moderate, corresponding to a dimensionless core mass-to-flux ratio $\lambda \sim 3\text{--}4$. This result is related to the magnetic flux problem, which lies at the heart of magnetized star formation. As mentioned in §1, if the magnetic flux of a typical dense star-forming core were to be carried into the central star, the stellar field strength would be orders of magnitude higher than the observed values (see, e.g., §4 of Nakano 1984). The vast majority of the core magnetic field must be decoupled from the central mass. What happens to the decoupled magnetic flux?

The decoupled flux can in principle be trapped by the protostellar accretion flow through ram pressure. For a simple estimate, we note that the magnetic flux associated with a stellar mass of M_* is given by $\Phi_* = 2\pi G^{1/2} M_*/\lambda$, where λ is the dimensionless mass-to-flux ratio of the star-forming core. If, after decoupling from the stellar mass, this flux

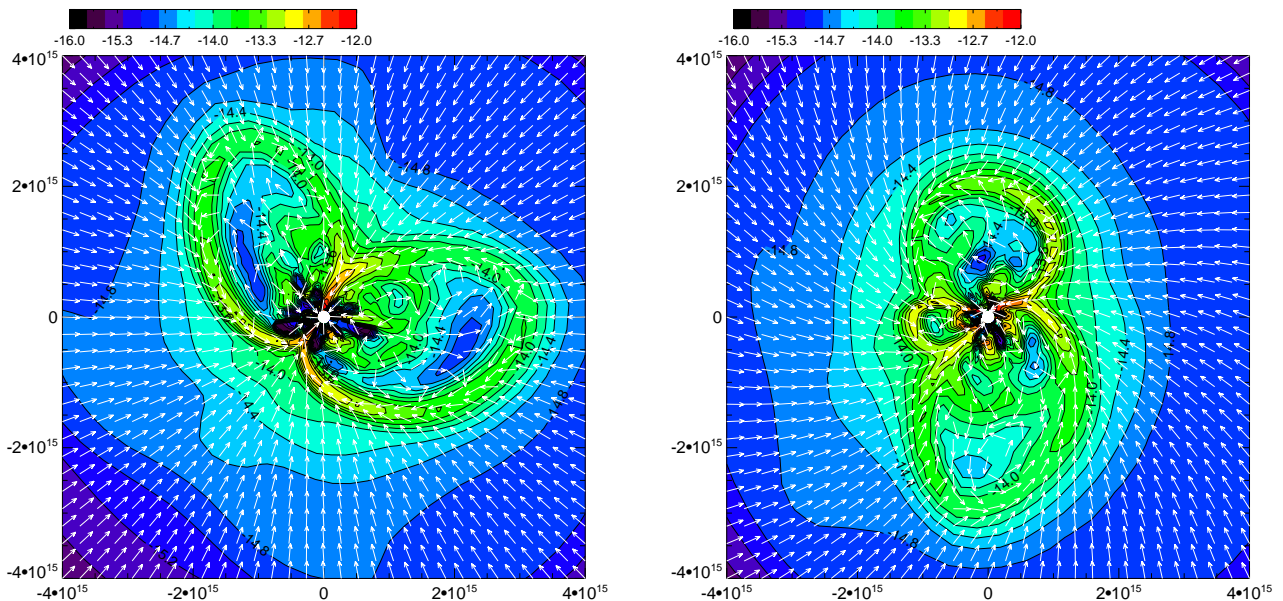


FIG. 8.— Distribution of the logarithm of the mass density ρ and velocity field (unit vectors) on the equatorial plane, for Models I (left panel, non-rotating) and J (right, rotating) that include both ambipolar diffusion and (enhanced) Ohmic dissipation for magnetic decoupling at small radii. Again, both models show filamentary structures in the inner protostellar accretion flow driven by magnetic interchange instability.

is confined within a (cylindrical) radius of R , the field strength inside the radius would be $B \approx \Phi_*/(\pi R^2)$, and the associated magnetic pressure would be

$$P_B \approx \frac{GM_*^2}{2\pi\lambda^2 R^4}. \quad (2)$$

This magnetic pressure is to be compared with the ram pressure of the protostellar accretion flow at the same radius

$$P_R = \rho v_r^2 \approx \frac{\sqrt{2}}{4\pi h} \frac{G^{1/2} M_*^{1/2} \dot{M}}{R^{5/2}}, \quad (3)$$

where \dot{M} is the rate of mass accretion (which occurs mostly through a dense, flattened pseudodisk), and h is the half-thickness of the pseudodisk relative to the radius R . The infall speed v_r is assumed to be close to the free fall speed $v_{\text{ff}} = (2GM_*/R)^{1/2}$. The ratio of the magnetic to ram pressure is therefore

$$\xi \approx \frac{\sqrt{2}hG^{1/2}M_*^{3/2}}{\lambda^2\dot{M}R^{3/2}} = 1.14 \times 10^2 \left(\frac{h}{0.1}\right) \left(\frac{M_*}{0.5M_\odot}\right)^{3/2} \left(\frac{4}{\lambda}\right)^2 \left(\frac{10^{-5}M_\odot\text{yr}^{-1}}{\dot{M}}\right) \left(\frac{10^{14}\text{cm}}{R}\right)^{3/2}. \quad (4)$$

Note that the magnetic pressure increases with decreasing radius faster than the ram pressure, indicating that it is more difficult to confine the decoupled flux to a smaller radius. For example, at the inner boundary of our simulation domain ($R = 10^{14}$ cm), the decoupled flux would produce a magnetic pressure larger than the ram pressure by two orders of magnitude for typical parameters; it cannot be confined there. The same is even more true if the inner edge of the simulation is chosen to be closer to the protostar. The decoupled flux must therefore expand to a region well beyond the inner boundary of our simulation. The characteristic size of the region can be estimated by setting the ratio ξ in equation (4) to 1 (see also Li & McKee 1996, their equation 9):

$$R_B \approx 2.35 \times 10^{15} \left(\frac{h}{0.1}\right)^{2/3} \left(\frac{M_*}{0.5M_\odot}\right) \left(\frac{4}{\lambda}\right)^{4/3} \left(\frac{10^{-5}M_\odot\text{yr}^{-1}}{\dot{M}}\right)^{2/3} \text{ cm}. \quad (5)$$

At this radius, the ratio of the magnetic to thermal pressure would be

$$\xi = 1.41 \times 10^2 \left(\frac{0.2\text{ km s}^{-1}}{a}\right)^2 \left(\frac{0.1}{h}\right)^{2/3} \left(\frac{\lambda}{4}\right)^{4/3} \left(\frac{\dot{M}}{10^{-5}M_\odot\text{yr}^{-1}}\right)^{2/3}, \quad (6)$$

which is much greater than unity for typical parameters. We therefore expect the decoupled magnetic flux to dominate the dynamics of the inner protostellar accretion flow up to R_B , if it can be transported outward to such a radius.

5.2. Two Modes of Magnetic Flux Transport: Microscopic Diffusion vs Macroscopic Advection

How the magnetic flux is transported outward against the collapsing inflow depends critically on the dimensionality assumed for the problem. In a 2D (strictly axisymmetric) collapsing flow, the flux can be transported outward only through microscopic non-ideal MHD processes, such as ambipolar diffusion or Ohmic dissipation, which allow the bulk material to cross the field lines. (We note that, in 2D ideal MHD simulations, magnetic diffusivity and reconnection of numerical origin can have a similar effect.) For realistic levels of cloud core ionization, the microscopic magnetic diffusion coefficient over most of the collapsing flow is rather small, however (see, e.g., Li et al. 2011). The magnetic flux dragged in by the collapsing flow can diffuse outward only slowly. As a result, most of it is confined to a small circumstellar region where the field strength is high and, in the case of ambipolar diffusion, the diffusion rate is enhanced by a large field gradient. The situation is analogous to the energy transport by radiative diffusion inside a star: for a small radiative diffusion coefficient (or a large Rosseland mean opacity), a large temperature gradient is required to transport a given energy flux. When the temperature gradient in a region becomes too large, the matter would turn convective, with energy advected outward by bulk fluid motions. If the star were to be held strictly spherically symmetric, this second mode of energy transport would be completely suppressed.

Similarly, we have demonstrated that, when the assumption of axisymmetry is lifted, the magnetic flux in a protostellar accretion flow can be transported outward by macroscopic advection as well. We showed that initially smooth axisymmetric protostellar accretion flows break up spontaneously, with the more strongly magnetized regions expanding away from the central gravitating object along some azimuthal directions and the less magnetized region sinking toward it along others. This simultaneous sinking and rising of material of different degrees of magnetization is a classical sign of the well-known magnetic buoyancy or interchange instability (e.g., Parker 1979; Kaisig et al. 1992; Stehle & Spruit 2001; de Gouveia Dal Pino et al. 2011). The flow pattern leads to an efficient outward transport of magnetic flux relative to matter, even in a region where the microscopic diffusion is absent (see §4).

5.3. Implications on Disk Formation

Our results have implications on a problem of considerable current interest: protostellar disk formation. For the observationally inferred level of magnetization in dense cores, disk formation is difficult in the strict ideal MHD limit, because a magnetic split-monopole is expected to form, which can remove essentially all of the angular momentum of the infalling material through magnetic braking (see discussion in §1 and references therein). Rotationally supported disks

are formed in some ideal MHD simulations (Machida et al. 2011), particularly when the rotation and magnetic axes are misaligned (Joos et al. 2012) or in the presence of a strong turbulence (Seifried et al. 2012, de Gouveia Dal Pino et al. 2011). However, the expected magnetic split-monopole is not clear in these calculations, which is a concern.

It was hoped that non-ideal MHD effects may weaken the magnetic braking enough to enable disk formation. Machida et al. (2007) and Dapp et al. (2012) showed that Ohmic dissipation can enable the formation of a small (AU-scale) rotationally supported disk (RSD) in a region where the column density is high enough to shield out the ionizing cosmic rays. Krasnopolsky et al. (2010) demonstrated that if the resistivity is significantly enhanced, it is possible to form even large, 100-AU sized RSDs. Such disks can also form in principle through spin-up caused by the Hall effect, if the Hall coefficient is large enough (Krasnopolsky et al. 2011). However, the microscopic values of the resistivity and Hall coefficient do not appear high enough for large RSDs to form (Li et al. 2011). Furthermore, ambipolar diffusion, the most widely studied non-ideal MHD effect in star formation, appears to make disk formation more (rather than less) difficult (see discussion in §1 and references therein). Classical non-ideal MHD effects may not enable disk formation, at least under the assumption of axisymmetry.

In the absence of axisymmetry, we find that the structure of the protostellar accretion flow is modified considerably by a new ingredient: interchange instability. This instability is expected to make disk formation easier, because it enables the magnetic flux accumulated near the protostar to be advected by the bulk fluid motions to a larger distance, which lowers the field strength (see Fig. 5) and thus the magnetic braking efficiency. However, we have carried out a number of simulations that include rotation (see Table 1), and found no evidence for the formation of a rotationally supported disk, even at relatively late times. This is in agreement with the AMR MHD simulations of Zhao et al. (2011), who noted that the strong magnetic field in the low-density expanding lobes prevents the rotating infalling material from making a full orbit around the center (see their Fig. 6 and the last panel in our Figs. 6 and 8). Our calculations indicate that the interchange instability in 3D may not weaken the magnetic braking enough to enable disk formation, although this issue deserves a closer examination.

Another implication is that, in the presence of interchange instability, ambipolar diffusion becomes less important in transporting magnetic flux. The reason is that the instability allows the magnetic flux to be advected outward, reducing the gradient in the field that is needed to drive the ambipolar diffusion. This result provides some justification for the 3D ideal MHD calculations of protostellar mass accretion, such as those of Zhao et al. (2011), that ignore ambipolar diffusion, as long as the magnetic decoupling at high densities is accounted for.

Finally, we mention in passing that the filamentary protostellar accretion flow structured by the interchange instability occurs on the scales of order 10^2 AU or larger, which can in principle be probed with the Atacama Large Millimeter/submillimeter Array in nearby star forming clouds. Observational studies of such a region may be important for understanding magnetized accretion onto not only protostars, but also other astrophysical objects, such as active galactic nuclei and the black hole at the Galactic center (e.g., Igumenshchev & Narayan 2002; Pang et al. 2011; McKinney et al. 2012).

5.4. Summary

We have carried out three dimensional simulations of the collapse of magnetized dense cores including three nonideal MHD processes: ambipolar diffusion, Ohmic dissipation, and decoupling at the inner boundary. Our main result is that the inner protostellar accretion flow is driven unstable by the magnetic flux decoupled from the matter that enters the central object. The instability is of the interchange type. When it is fully developed, the flow structure becomes highly filamentary, as a result of the interplay between gravity driven infall and magnetically driven expansion. We showed, in particular, that the magnetically-dominated structure inside the ambipolar diffusion-induced hydromagnetic shock found in previous axisymmetric studies is unstable in 3D, as it has been anticipated for some time. Without the restriction of axisymmetry, the redistributed magnetic flux can be transported outward advectively, through the bulk motions of low-density expanding regions. This new channel of efficient flux transport renders the microscopic processes, such as ambipolar diffusion, less directly important in redistributing magnetic flux in the protostellar accretion flow. It also lowers the magnetic field strength close to the protostar, which could in principle make the magnetic braking less efficient and the formation of a rotationally supported disk easier. However, we find no evidence for disk formation in any of our rotating collapse simulations. How a rotationally supported disk forms in a largely magnetically dominated, filamentary protostellar accretion flow is an outstanding unsolved problem.

The work was supported in part by NASA through NNX10AH30G and by the Theoretical Institute for Advanced Research in Astrophysics (TIARA) under the CHARMS initiative and the National Science Council of Taiwan through grant NSC97-2112-M-001-018-MY3.

REFERENCES

- Allen, A., Li, Z.-Y., & Shu, F. H. 2003, *ApJ*, 599, 363
 Braiding, C. R., & Wardle, M. 2012, *MNRAS*, 422, 261
 Ciolek, G. E., & Königl, A. 1998, *ApJ*, 504, 257
 Dapp, W. B., Basu, S., & Kunz, M. W. 2012, *A&A*, 541, A35
 Davidson, J. A., Novak, G., Matthews, T. G., Matthews, B., Goldsmith, P. F., Chapman, N., Volgenau, N. H., Vaillancourt, J. E., & Attard, M. 2011, *ApJ*, 732, 97
 de Gouveia Dal Pino, E. M., Leão, M. R. M., Santos-Lima, R., Guerrero, G., Kowal, G., & Lazarian, A. 2011, arXiv:1112.4871
 Duffin, D. F., Pudritz, R. E., Seifried, D., Banerjee, R., & Klessen, R. S. 2011, arXiv:1111.5375
 Goodman, A. A., Benson, P., Fuller, G. A., & Myers, P. C. 1993, *ApJ*, 406, 528
 Galli, D., Lizano, S., Shu, F. H., & Allen, A. 2006, *ApJ*, 647, 374

- Galli, D., & Shu, F. H. 1993, *ApJ*, 417, 243
- Girart, J. M., Rao, R., & Marrone, D. P. 2006, *Science*, 313, 812
- Hennebelle, P., & Fromang, S. 2008, *A&A*, 477, 9
- Igumenshchev, I. V., & Narayan, R. 2002, *ApJ*, 566, 137
- Joos, M., Hennebelle, P., & Ciardi, A. 2012, arXiv:1203.1193
- Kaisig, M., Tajima, T., & Lovelace, R. V. E. 1992, *ApJ*, 386, 83
- Krasnopolsky, R., & Königl, A. 2002, *ApJ*, 580, 987
- Krasnopolsky, R., Li, Z.-Y., & Shang, H. 2010, *ApJ*, 716, 1541
- Krasnopolsky, R., Li, Z.-Y., & Shang, H. 2011, *ApJ*, 733, 54
- Kunz, M. W., & Mouschovias, T. Ch. 2010, *MNRAS*, 408, 322
- Li, Z.-Y., Krasnopolsky, R., & Shang, H. 2011, *ApJ*, 738, 180
- Li, Z.-Y., & McKee, C. F. 1996, *ApJ*, 464, 373
- Lubow, S. H., & Spruit, H. C. 1995, *ApJ*, 445, 337
- Machida, M. N., Inutsuka, S., & Matsumoto, T. 2007, *ApJ*, 670, 1198
- Machida, M. N., Inutsuka, S., & Matsumoto, T. 2011, *PASJ*, 63, 555
- Matthews, B. C., McPhee, C. A., Fissel, L. M., & Curran, R. L. 2009, *ApJS*, 182, 143
- McKinney, J. C., Tchekhovskoy, A., & Blandford, R. D. 2012, arXiv:1201.4163
- Mellon, R. R., & Li, Z.-Y. 2008, *ApJ*, 681, 1356
- Mellon, R. R., & Li, Z.-Y. 2009, *ApJ*, 698, 922
- Nakano, T. 1984, *Fundamentals of Cosmic Physics*, vol. 9, 139
- Nakano, T., & Nakamura, T. 1978, *PASJ*, 30, 671
- Nakano, T., Nishi, R., & Umabayashi, T. 2002, *ApJ*, 573, 199
- Padovani, M., Galli, D., & Glassgold, A. E. 2009, *A&A*, 501, 619
- Parker, E. N. 1979, *Cosmical Magnetic Fields, their origin and activity*. (Oxford: Clarendon Press), ch. 15
- Pang, B., Pen, U.-L., Matzner, C. D., Green, S. R., & Liebendörfer, M. 2011, *MNRAS*, 415, 1228
- Ramsey, J. P., Clarke, D. A., & Men'shchikov, A. B. 2012, *ApJS*, 199, 13
- Seifried, D., Banerjee, R., Klessen, R. S., Duffin, D., & Pudritz, R. E. 2011, *MNRAS*, 417, 1054
- Seifried, D., Pudritz, R. E., Banerjee, R., Duffin, D., & Klessen, R. S. 2012, *MNRAS*, 422, 347
- Shu, F. H. 1992, *The Physics of Astrophysics, Vol. II* (Sausalito: University Science Books)
- Shu, F. H., Laughlin, G., Lizano, S., & Galli, D. 2000, *ApJ*, 535, 190
- Spruit, H. C., & Taam, R. E. 1990, *A&A*, 229, 475
- Stehle, R., & Spruit, H. C. 2001, *MNRAS*, 323, 587
- Troland, T. H., & Crutcher, R. M. 2008, *ApJ*, 680, 457
- Ward-Thompson, D., Kirk, J. M., Crutcher, R. M., Greaves, J. S., Holland, W. S., & André, P. 2000, *ApJ*, 537, 135
- Wang, P., & Abel, T. 2009, *ApJ*, 696, 96
- Zhao, B., Li, Z.-Y., Nakamura, F., Krasnopolsky, R., & Shang, H. 2011, *ApJ*, 742, 10